FlexCube

A flexible multimodal haptic display

MSc. Thesis

Khoa Lanh Luu Anh

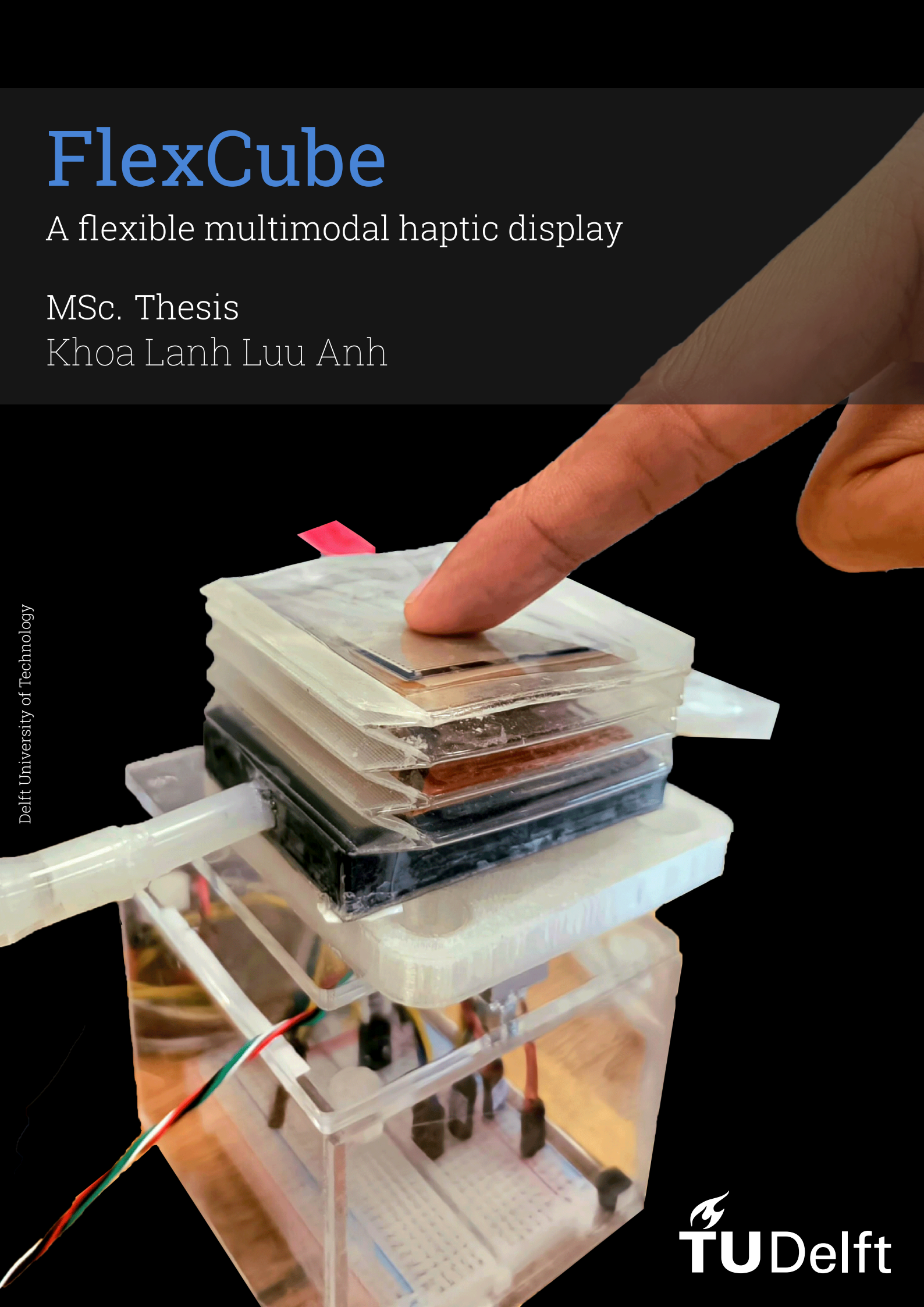

Delft University of Technology

TU Delft

FlexCube

A flexible multimodal haptic display

by

Khoa Lanh Luu Anh

Student Name	Khoa Lanh Luu Anh
Student Number	5699622

Supervisor: Prof. Yasemin Vardar
Haewon Jeong

Faculty: Faculty of Mechnical Engineering, Delft

Thesis Committee: Prof. Yasemin Vardar
Haewon Jeong
Prof. Mohammad J Mirzaali
Prof. Barys Bhyrokau

TU Delft

Preface

”To those who have guided and supported me on this journey, I offer my deepest gratitude. Without you, I would not have made it this far, and your place in my heart is forever secure.”

To Professor Yasemin, thank you for believing in my ability and challenging me with a project that pushed my boundaries. I am really sorry about all the hardships we have faced in our communication. This will be my biggest regret regarding the time I worked on this project; I wish I could have fixed it somehow. Thank you so much, for not giving up on me after all. Your guidance has been invaluable, and your trust in me has given me the confidence to pursue my goals.

To Haewon, my daily supervisor, thank you for all the tiny but great tips and instructions you have always given me throughout the whole time we worked together. Thank you for being understanding and super helpful whenever I am in trouble. I wish you all the best in your next journey, and I hope we still have a chance to work together in the future.

To all my labmates, thank you for all your constant support, both professionally and mentally, whether it was through the brainstorming sessions, the times we hung out together, or simply the time we shared a laugh during lunchtime.

And to a special friend, Hanan, thank you for being here, being my anchor. Your encouragement, understanding, and support have been my strength, especially during the most difficult times. Your presence in my life is a gift that I cherish deeply.

Lastly, I must thank my family for their unwavering support from 10000 km away. Thank you for always keeping the flame of hope burning in me ...

Khoa Lanh Luu Anh

Contents

1

Paper

FlexCube: A flexible multimodal haptic display

Khoa Lanh Luu Anh[569962], Haewon Jeong, Yasemin Vardar
Delft University of Technology, Delft, The Netherlands

***Abstract*—As virtual technology rapidly advances globally, the integration of the sense of touch into virtual environments to enhance realism is becoming increasingly urgent, drawing significant attention from scientists and researchers. This has led to the development of innovative haptic devices designed to replicate tactile sensations, further immersing users in virtual experiences. However, despite significant research in this field, most of the current haptic devices appear to lack the ability to provide direct, flexible, and natural interactions. To address these challenges, this study introduces the FlexCube, a novel flexible multimodal haptic display capable of delivering three tactile sensations: softness, roughness, and temperature. The FlexCube is developed through the creation of two modules—a hydraulic-actuated module for temperature and contact area rendering and a roughness module using the electrovibration effect. Then, they are combined together and integrated with an available stiffness rendering device into one device - the complete FlexCube. Subsequent experiments were conducted to evaluate the performance and behavior of each module individually. The results demonstrate that the FlexCube is capable of rendering a step profile and real texture's temperature profile, tracking a sinusoid contact area profile of 0.2 Hz with neglectable delay, and able to deliver salient roughness sensations with the maximum generated electrovibration force of 0.028N regardless of the possible surface deformation. Overall, the FlexCube can simultaneously deliver all the expected tactile sensations and appears to be a promising tool for applications in E-commerce, telepresence, and interactive simulations.**

***Index Terms*—Tactile perception, Multimodality haptic display, soft haptic display**

I. Introduction

Nowadays, with the rapid development of virtual reality (VR) technology, the limit of human vision seemingly does not exist anymore. VR can help us visually travel everywhere while physically just staying in one place, without any constraints of distance, time, or even the reality of the destination. However, human beings, with 5 senses to perceive the surrounding world every day, need more than just visual information to achieve realistic feelings. Among those 5, vision and hearing are considered major senses due to the highly valuable information they bring to us. Meanwhile, touch, despite being a major sense, appears to be the most active and plays an important role in constituting a realistic sensation. While devices that deliver vision (VR glasses) and hearing (speakers, headphones) cues are already popularly available, the regeneration of virtual tactile sensation is still in the developing phase.

One of the biggest challenges of delivering a virtual tactile feeling is the multimodal nature of touch. This sense integrates multiple types of sensory information to create a comprehensive perception of the environment. Unlike other senses that primarily rely on a single type of stimulus (like vision relying on light or hearing on sound waves), touch involves various types of sensory receptors that detect different stimuli consisting of many different sensations (such as hot/cold, rough/smooth, sticky/slippery, etc.). Therefore, to regenerate the sense of touch, the created devices, which are generally called multimodal haptic devices, are required to be capable of giving as many tactile sensations as possible.

Much research has been immersed into this field with the generation of many multimodal devices using different working principles and in different forms. Some researchers designed a wearable haptic device that is installed on the hands or arms of users, such as a glove [1][2], a forearm cover [3][4], or a ring [5][6]. Meanwhile, other researchers focused on making a tool-based haptic device, which requires a more active interaction from the users to hold and move the hand-held tool around. Some prominent products of this category are the stylus-based [7]–[10], computer mouse-based [11]–[13], manipulator-based [14]–[16].

Although wearable and tool-based devices are generally simpler to manufacture and easier to modulate the rendered sensations, there is a widespread preference from users for a natural and direct interaction with bare fingers in terms of perceiving a virtual texture. This tendency leads to a big concern from scientists and engineers in making a display-based device that contains a flat, controllable and property-adjustable surface. Several achievements have been made in creating this type of direct-interaction haptic display [17]–[20]. However, the biggest drawback of those devices is the rigid form of the touch display. The main reason is that most of the mechanisms applied to render tactile sensations in previous research relate to the use of hard materials. For example, in [17], [18], [20], the authors use the Peltier element to render thermal cues, which is usually made from ceramic to ensure good electrical insulation properties. In [19], on the other hand, the author utilizes a commercial touch screen and turns it into an electrovibration display to generate the vibration sensation. In general, the use of popular and available components appears to have hindered the creation of a more flexible tactile display. Overall, soft multimodal haptic devices were significantly understudied due to several practical reasons. Moreover, integrating hand-made components instead of using standardized and commercialized ones is much more challenging since we can not fully anticipate the behavior of those DIY (do it yourself) products. This, apparently, is a fair trade-off for the potential of creating a unique flexible display that can deliver similar tactile sensations compared to the current rigid display.

Therefore, in this research, we delve into creating a new flexible multimodal haptic display, the **FlexCube**, which is

capable of delivering 3 tactile sensations: softness, roughness, and temperature. The Flexcube is created by first designing and building two modules:*Hydraulic-actuated module* (for temperature and contact area rendering) and *Roughness module* (for roughness rendering). The operations of these two modules are then inspected separately before combining them together into one system. Finally, the combined system is integrated into a stiffness rendering device, which was previously available in the Haptic Interfaces Technology Lab (HITLAB), to create a complete multimodal haptic display - the FlexCube. Also, it is important that the selected rendering mechanisms in the two added modules allow high flexibility for the entire display structure. In section II, a brief background regarding 3 rendered tactile perceptions (roughness, softness, and temperature) is demonstrated, followed by the working principle of the utilized stiffness rendering device. Section III outlines the design process for the FlexCube, highlighting the working principles of the hydraulic and roughness modules. In section IV, the characteristics of each subsystem are investigated by conducting several characterization experiments, which eventually give us useful insight into the behaviors of the FlexCube. Finally, in section V, a discussion is made on the findings relating to both hydraulic and roughness modules, followed up by some future work plans and recommendations.

II. Background

A. Perception of Roughness

The perception of roughness, which mainly relates to the sliding motion of the finger, is detected by the 3 mechanoreceptor types: Meissner's corpuscles, Merkel cells, and Ruffini endings. Meissner's corpuscles are particularly sensitive to light touch and vibrations, playing a significant role in detecting rough surfaces.

Among the various attributes that characterize surface textures, roughness is one of the most extensively studied due to its significant impact on both the physical and perceptual qualities of surfaces [21], [22]. The tactile perception of roughness is fundamentally a spatiotemporal process that involves both spatial and temporal cues from skin indentation and vibration, respectively [23]. During finger exploration, the spatial distribution of surface features such as bumps and grooves is detected by the skin's indentation on the fingers, enabling the discrimination of macro roughness of macrotextures. Meanwhile, for microtextures, the perception relies more on vibratory (and therefore temporal) stimuli, which is usually addressed as vibrotactile sensation [24].

The current haptic devices use various technologies to replicate roughness, such as vibrotactile (with small vibration motors or piezoelectric actuators) [6][25][26], electrovibration (modulating electrostatic forces between the device and the user's skin to create sensations of friction and texture changes) [27]–[30], or surface actuation (arrays of small actuators deform the surface of the device to create bumps and grooves) [31]–[33]. The resulting virtual textures also highly depend on the stimulus delivered. In specific, a high-amplitude (equivalent to high skin indentation) and low-frequency stimulus will give a macro-roughness sensation, while low-amplitude and high-frequency stimulus can provide a micro-roughness feeling.

B. Perception of Softness

The sensation of softness when interacting with an object is often associated with the pushing and tapping movements of the finger. Softness perception involves both cutaneous and kinesthetic cues, which combine to help us determine how soft or firm an object is [34].

Cutaneous cues are the sensory signals received from the skin and are detected by 2 mechanoreceptors: Meissner's corpuscles and Merkel cells, which are sensitive to light touch and pressure. These cues give us information about the skin deformations such as skin stretch or skin indentation when we touch an object. Kinesthetic cues, on the other hand, are the sensory signals received from muscles, tendons, and joints, which provides information about the position, movement, and the force applied by the finger.

The sensory information received from the kinesthetic cues and cutaneous cues are directly related to 2 physical quantities: object's stiffness and touch contact area respectively [35]. When we push a surface, the muscles and tendons in our fingers sense the force we are applying and how much the object is deforming, which informs us about its stiffness property. However, a complete sensation of softness requires the information of the skin deformation of our finger when touching an object. A compliance material's surface will deform more when we apply a pushing force, leading to a larger wrapping contact area around the finger. Thanks to the contact area, we can distinguish between pushing a piece of metal placed on top of a spring versus pushing a real soft material such as a piece of foam.

Currently, haptic devices employ a wide range of advanced technologies to render the sensation of softness. These devices usually utilize force feedback actuators, such as electromagnetic[36][37], piezoelectric [38], pneumatic [35][39][40], and hydraulic actuators [41], to stimulate the resistant force felt when pushing the virtual objects.

C. Perception of Temperature

The perception of thermal sensations through touch primarily involves detecting temperature changes in the skin, which is detected by thermoreceptors: warm receptors and cold receptors. These thermoreceptors are embedded in the skin and respond to temperature fluctuations, providing information about the thermal properties of objects in contact. Warm receptors are most responsive to temperatures in the range of 30-45°C, while cold receptors are sensitive to temperatures between 10-27°C. Temperatures below 10°C or above 45°C are often perceived as painful rather than simply cold or warm.

The perception of temperature is influenced by both the material properties of the object and the thermal conductivity of the skin. Materials with higher thermal conductivity, such as metals, can quickly transfer heat to or from the skin, leading to a stronger and more immediate thermal sensation. In contrast, materials with low thermal conductivity, like wood or plastic,

produce more subtle temperature changes, leading to weaker thermal sensations.

Current haptic devices aim to replicate thermal sensations using various technologies. The most popular option is applying thermoelectric devices [7][42]–[44], which use the Peltier effect and can create localized heating or cooling by passing an electric current through a thermoelectric material. Another widely-used method is utilizing microfluidic systems [45]–[47] in which the warm or cool fluids are circulated through small channels within the device, offering localized and dynamic thermal feedback.

D. Available Stiffness rendering device

The available stiffness rendering device at HITLAB, which has an origami structure, is capable of stimulating different levels of stiffness by using a pneumatic system. As demonstrated in Fig. 1, the device consists of 3 main components: a 1-DOF origami joint that can only move vertically, a pouch motor placed inside the origami joint, and an origami bellows covering every other component from the outside. The main working principle is that when the pouch motor is inflated or deflated, it will respectively push up or push down the origami joint vertically. By modulating the pressure inside the pouch motor, different values of stiffness can be obtained.

To render a desired stiffness value, it is necessary to know the current force being applied by the user on top of the device and the resulting displacement of the top surface with respect to the base. By using a magnet installed on the movable top surface and a Hall sensor installed at the base, the relative displacement of the top surface can be measured. Also, a Force-sensing resistor (FSR) sensor is attached to the top of the origami joint which is responsible for measuring the force applied by the user. In operation, when a target stiffness value is given, we use the recorded data of the current indentation distance and multiply it with the desired stiffness to obtain the target force. Then, the pouch motor will be inflated or deflated to generate a force such that the net force between the user's pushing force and the force generated by the pouch is equal to the target force. During operation, the device needs to be connected to an air compressor to provide enough pressure, which is used to control the pouch.

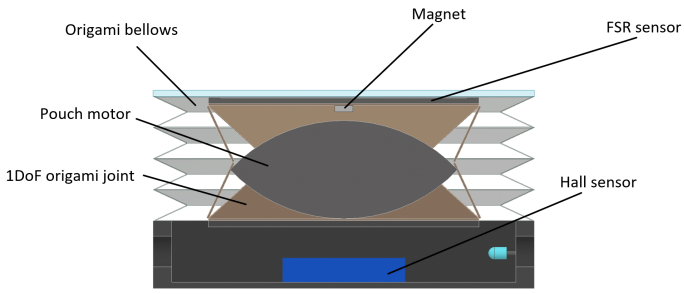

Fig. 1: Constitution of the 1-DOF stiffness rendering device.

III. Device Design

With the goal of creating a multimodal haptic display that can simultaneously deliver 3 tactile perceptions (softness, roughness, and temperature), the design process needs to take into account the possible interference of the mechanisms utilized to stimulate each modality to ensure the independence of the rendered stimuli. Apart from that, the device must be flexible (deformable) to maximize the user's realistic touch sensation. Finally, compatibility is another important factor that needs to be considered since the added components have to be easily integrated and not obstruct the operation of the available stiffness rendering device.

With all those considerations, the FlexCube was designed with the base is the available stiffness-rendering device (Pneumatic module) and 2 add-on modules: *Hydraulic module* and *Roughness module*. The *Hydraulic module* is responsible for both delivering thermal sensation and adjusting the touch contact area, while the *Roughness module* generates the roughness sensation. In this section, the working principle, materials, and components utilized in each add-on module will be demonstrated. The overall system is shown in Fig. 2, while the signal workflow between the hardware components is depicted in Fig. 3. The microcontroller units utilized in this research are two Teensy 4.1 development boards. As depicted in Fig. 3, during operation, the *Master* Teensy is directly connected with the PC to receive the command and send back the data recorded by all sensors. At the same time, *Master* Teensy receives data from all the thermistors and loadcells while giving commands to all the drivers and relays. It also sends the control voltage signal to the *Roughness module* via the NI-DAQ unit as well as receives the compass sensor and FSR sensor data from the *Slave* Teensy. Meanwhile, the *Slave* Teensy is responsible for controlling the pneumatic valve and receiving data from the FSR sensor, compass sensor, and pressure sensors.

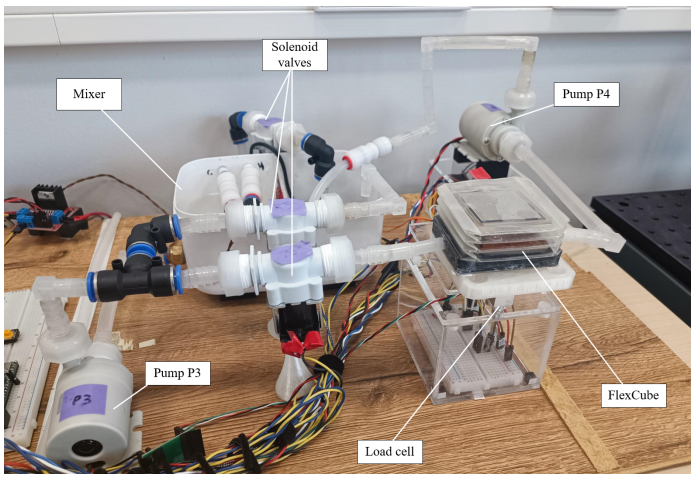

Fig. 2: The overall system experimental setup.

A. Hydraulic Module

A closed-circuit hydraulic-actuated system is designed to conduct a flow of temperature-modulated and flow rate-modulated fluid passing through the FlexCube. The liquid used in the system is water, which has a high specific heat

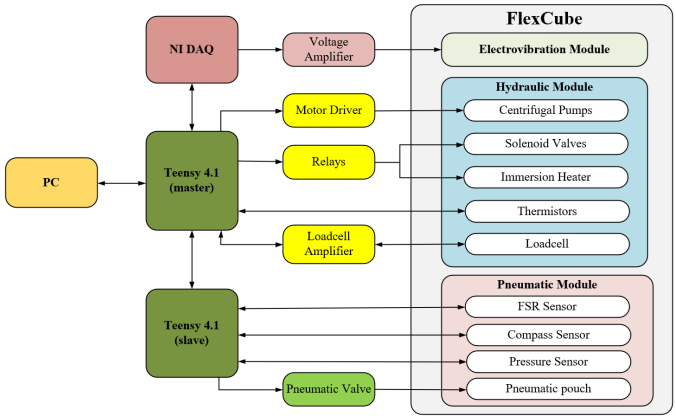

Fig. 3: The signal workflow between the hardware and the software interface.

capacity, therefore enabling stable heat transfer capability and ensuring no blockage occurs in the pipeline and other components during operation. The overall schematic of the hydraulic system utilized is shown in Fig. 4.

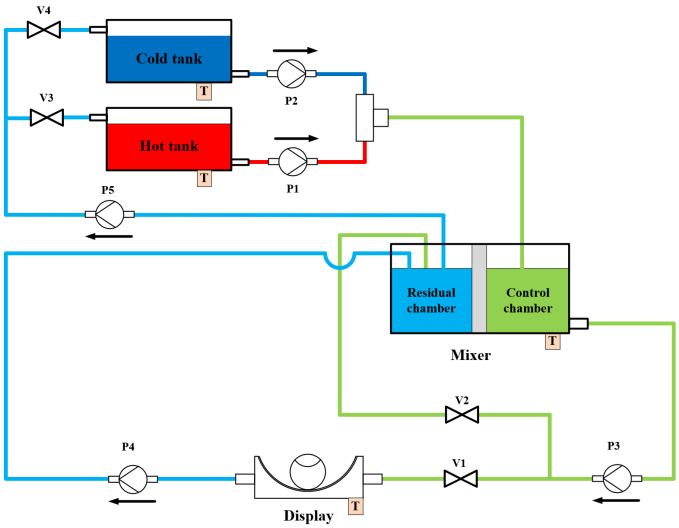

Fig. 4: Schematic of hydraulic system.

This module consists of three water tanks, namely *Hot tank*, *Cold tank*, and *Mixer*. Three NTC thermistors (TRU COMPONENTS MJSTS-103-3950-1-600-3D) are used to measure the temperature of the water in all three tanks. The maximum volumes of both the *Hot* and *Cold tank* is 2 liters, while the *Mixer* is divided into two 300ml chambers, called *Control chamber* and *Residual chamber*. The large volume of the *Hot* and *Cold tank* are necessary to mitigate the effect of the returning flow's temperature. In other words, the larger the tanks, the more stable their temperatures are. However, this is also a trade-off since using a bigger tank will require more time to heat up or cool down the water inside at the beginning of each experiment. The water in the *Hot tank* is heated up by using a 300W immersion heater (WIGO RTE 304) and maintained at 40^oC by a simple pair-wise control algorithm. The *Cold tank*, on the other hand, is a 120W Ice Maker (PRIMO PR407IB) in which the ice is continuously generated to maintain the temperature of 10^oC of the water inside. The flow of water is motivated by 5 centrifugal pumps (Bayite BYT-7A006) and directed by 4 solenoid valves (W-PM422 Whadda).

For the temperature rendering task, the main goal is to achieve a certain volume of water with a targeted temperature inside the *Control chamber* before pushing that water through and filling up the FlexCube so that the user can perceive the water temperature when touching the FlexCube's top surface. During operation, the water from the *Hot* and *Cold tank* is firstly pumped towards the *Control chamber* by using two separately controlled pumps (**P1** and **P2**). The two streamlines are merged with a T-shaped connector before being directed into the *Control chamber*. By adjusting each pump's speed, corresponding to the speed of each water stream flowing from the *Hot* and *Cold tank*, different temperatures of the mixed stream can be obtained before reaching the *Control chamber*. An NTC thermistor installed inside the *Control chamber* will measure the temperature of the current water volume at every instant and feed the signal back for the controller to modulate the pumps' speed if necessary.

Another pump (**P3**) is installed at the outlet of the *Control chamber* in order to direct the water out of the *Mixer* and ensure the water level in the *Control chamber* is as low as possible. The low level of water inside the *Control chamber* will significantly improve the control accuracy and response time since the temperature of the incoming mixed stream is less affected by the temperature of the water already present in the chamber. Besides, two solenoid valves (**V1** and **V2**) are installed at the outlet side of pump **P3**, dividing the streamline into 2 branches, one leading to the FlexCube, and one heading back to the *Residual chamber* of the *Mixer*. These two valves are activated alternately to direct the flow from pump P3, either toward the FlexCube to start rendering the thermal cues or back into the *Residual chamber* during the standby period when we need to wait until achieving the desired temperature for the water inside the *Control chamber*.

For the contact area rendering task, the idea is to change the size of the area of the FlexCube's top surface contacting the finger during the interaction by changing the water volume inside the origami bellows. As demonstrated in Fig. 5, with a certain indentation of the user's finger, increasing the water volume will deform the FlexCube's top surface, wrapping up more area of the finger and therefore increasing the contact area sensation.

To realize such a working principle, another pump (**P4**) is installed at the outlet of the FlexCube to control the flow rate of the stream flowing out. Together with pump **P3**, the speeds of these two pumps are separately controlled to generate 3 possible states for the control strategy:

- When the inflow speed is larger than the outflow speed ($Q_{in} > Q_{out}$): The water volume increases, leading to the increase of the contact area.
- When the inflow speed is smaller than the outflow speed ($Q_{in} < Q_{out}$): The water volume decreases, leading to

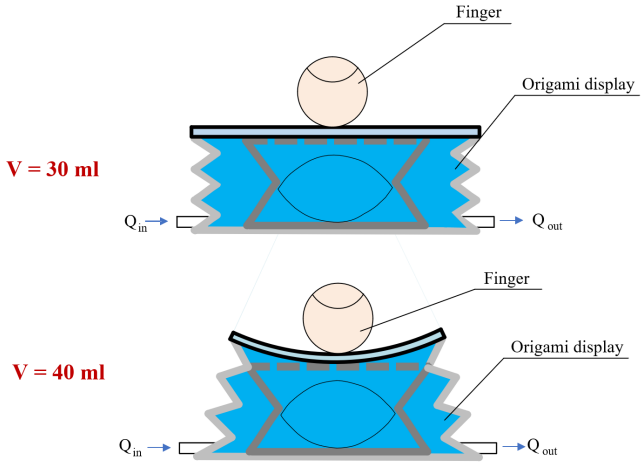

Fig. 5: Illustration of the contact area control strategy.

the decrease of the contact area

- When the inflow speed is equal to the outflow speed ($Q_{in} = Q_{out}$): The water volume is kept unchanged, maintaining the contact area at the current state.

Theoretically, the volume of water inside the FlexCube can be determined and computed from the speeds of inflow and outflow by applying the integration formula:

$$V = \int_{t_1}^{t_2} (Q_{in} - Q_{out})\, dt = (Q_{in} - Q_{out})\, \Delta t \qquad (1)$$

In practice, the measurement and control of the flow speed are much more challenging since most flow sensors have a considerably long delay time before giving a precise flow rate result. Therefore, we determined the water volume via the water's weight, which was measured by a load cell installed under the FlexCube. During the user's interaction, the resulting values obtained from the load cell, however, can be affected by the pushing force exerted by the user's finger. To compensate for that, we utilized the FSR sensor, which was attached on top of the foldable 1-DOF origami structure inside the FlexCube, to measure the finger's pushing force so that we could exclude that force from the results given by the load cell.

The returning flow from the FlexCube is directed back to the *Residual chamber* of the *Mixer* before being pumped back to either the *Hot* or *Cold tank* by pump **P5**. Two other valves (**V3** and **V4**) are installed at the outlet of pump **P5**, which are utilized to control the distribution of the stream flowing back to either the *Hot* or *Cold tank*. In short, if the rendering temperature is hotter than a certain threshold (chosen as 30^oC), the valve leading to *Hot tank* (**V3**) will be activated (opened), and vice versa. This small control strategy helps stabilize the water temperatures in those two tanks and keep them unchanged for longer, taking less time to wait for them to go back to the initial temperatures (40^oC for hot and 10^oC for cold).

B. Roughness Module

The roughness module is a thin transparent film attached to the top of the FlexCube by silicone glue. The main working principle of this module is applying the electroadhesion phenomenon to generate a virtual roughness sensation. Electroadhesion is defined as an attractive force occurs between two contacting materials when there is an electrical potential difference between them [48], where ε_0 is the vacuum permittivity, A is the finger contact area, d_i and d_{SC} are the thicknesses of the insulator and the stratum corneum and ε_i and ε_{SC} are the relative permittivities of the insulator and stratum corneum. Based on that, the electrovibration effect occurs when humans touch or slide their fingers on an insulated electrode being applied with an alternate voltage. The result is the creation of a haptic sensation of roughness due to the alternate electrostatic force attracting and releasing our finger skin periodically. The application of this effect to generate a virtual roughness sensation has been implemented in plenty of research before. However, as mentioned in Section I, the use of commercial touchscreens for this work made the integration of a softness rendering function impossible. To realize the rendering mechanism of the contact area in Section III.A, a flexible/bendable electrovibration display must be created, which needs to be thin enough to be able to deform under the finger's pressing forces as well as not obstruct the heat transfer from the water flow below.

All things considered, a thin film is designed with one conductive layer as a base and one insulating layer on top as an insulator. It is also noteworthy that the magnitude of the electrovibration force is proportional to the insulator's dielectric constant and inversely proportional to the square of the insulator's thickness, as shown in Eq. 2 [49]. The materials of both conductive and insulating layers should have high thermal conductivity so as not to obstruct the heat transmission between the water inside the FlexCube and the user's finger on the top surface. In this research, we decided to use ITO film as a conductive layer with $50um$ thickness and UV-cured Epoxy Resin as the insulator (refer to the work in [50]). The properties of these two material are given in Appendix [B].

$$F_e = \frac{\varepsilon_0 A V^2}{2\left(\frac{d_i}{\varepsilon_i} + \frac{d_{SC}}{\varepsilon_{SC}}\right)(d_{SC} + d_i)} \qquad (2)$$

Since insulator thickness plays a significant role in the generation of the electrovibration effect, we decided to use the spin-coating method to coat a thin layer of Epoxy Rein onto the ITO film. This method is chosen because it has the huge advantage of simplicity, quickness, and ensuring a uniform coating layer. Also, the coating thickness can be modulated effectively by adjusting the spinning speed and time. During our manufacturing process, we added Acetone as a thinner of Epoxy Resin to decrease the viscosity of the solution so that we could obtain the thinner coating layer. The spin-coating recipe implemented is also included in Appendix [B]. The resulting coated film is shown in Appendix [D]. To connect the conductive layer with the power supply, we keep one corner of the ITO film uncoated and connect a connector into that area.

The coating thickness is measured by using a microscope to observe the polished cross-section of the sample. The image captured from the microscope is shown in Fig. 6. It can be

seen that the thickness of the coated layer is approximately $6um$. The uniformity of the coating thickness is also inspected by visualizing the cross-section images at different positions on the coated film. The resulting images (Appendix [D]) show that the coating thickness varies from $5-6um$. This $1um$ thickness deviation can lead to different intensities of roughness perception by the user. To circumvent this problem, we can instruct the users to mainly move their fingers near the center of the film where the coating thickness is higher but distributes more uniformly. The finished electrovibration film is finally attached to the top of the FlexCube by glue to prevent leakage from the water from inside.

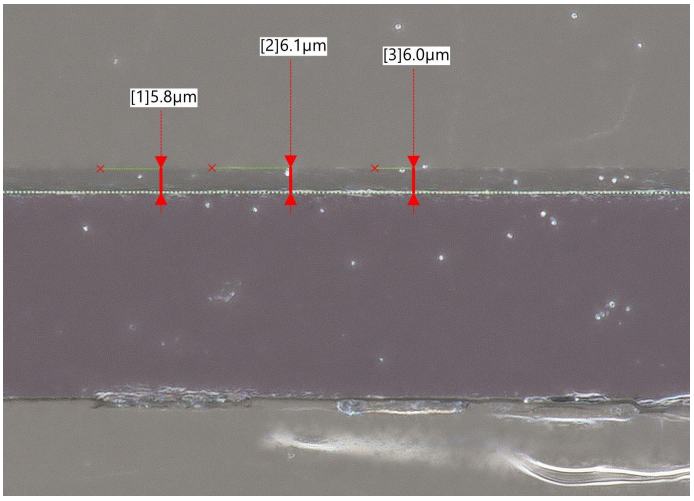

Fig. 6: Cross-section image of the resin electrovibration layer ($6\mu m$.)

IV. Device Characterization

In this section, the characteristics of two modules (*Hydraulic* and *Roughness*) with three tactile modalities (thermal, contact area, and roughness) are inspected. The obtained results will give us insight into the performance quality, working limit, and response time of the FlexCube, which is essential and beneficial for the future human experiment phase.

A. Thermal rendering characteristics

The temperature stimuli delivered by the FlexCube are expected to range from 10^oC to 40^oC, which falls into the comfort range of humans so that we can ensure a pleasant sensation for users during the interaction. The temperature of the mixed stream (T_{mixed}), which is also the rendered temperature by the FlexCube, depends on the temperatures of the *Hot tank* (T_{hot}) and *Cold tank* (T_{cold}), and on the flow speed of the streams from those two tanks (Q_{hot} and Q_{cold}). That relation can be seen in the following formula:

$$T_{mixed} = \frac{Q_{hot}T_{hot} + Q_{cold}T_{cold}}{Q_{hot} + Q_{cold}} \tag{3}$$

During the stimulation process, two temperature values at two positions along the streamline are measured, which are the ***Mixer temperature*** and ***Display temperature***. *Mixer temperature* is the water temperature inside the *Control chamber* which directly results from the mixing of two flows from the *Hot* and *Cold* tanks. *Display temperature*, on the other hand, is the water temperature inside the FlexCube. Since the FlexCube is, in practice, installed $60cm$ away from the *Mixer* along the pipeline, *Display temperature* is expected to show a considerable delay compared to *Mixer temperature*. Moreover, the *Display temperature* can be varied due to the heat transfer from the water flowing inside to the user's finger touching the top surface during the interaction.

Since the intended stimuli duration is short ($15s$), the values of T_{hot} and T_{cold} can be assumed to be unchanged during the interaction process. Hence, T_{mixed} (*Mixer temperature*) can be completely controlled by adjusting the values of Q_{hot} and Q_{cold}, which are directly proportional to the PWM signal sent to the corresponding pumps. It is noteworthy that the PWM signals controlling two pumps (P1 and P2) are coupled via an intermediate variable, called $input$, ranging from 0 to 1023. The relationship between them is shown below:

$$PWM1 = input\left(\frac{UB1 - LB1}{1023}\right) + LB1 \tag{4}$$

$$PWM2 = input\left(\frac{LB2 - UB2}{1023}\right) + UB2 \tag{5}$$

In which indexes 1 and 2 indicate the hot and cold sides respectively, while UB and LB are upper bound and lower bound values of the PWM control signal that can activate the pumps. The variations of $PWM1$ and $PWM2$ with respect to different values of $input$ are demonstrated in Fig. 7 (upper). Also, the resulting rendered temperatures (both *Mixer* and *Display*) corresponding to those variations are shown in Fig. 7 (lower). It can be seen that the higher value of $input$ will result in higher stimulated temperatures. By using this control strategy, we can simultaneously vary the speeds of two pumps inversely, which helps accelerate the changing rate of T_{mixed}. The variable of $input$, then, can be considered as a single input signal for the temperature rendering subsystem, while the *Display temperature* is the single output.

Overall, the measurements of both temperatures are necessary and important for the control process. Specifically, *Mixer temperature* shows a much faster response, which gives precise information about the mixed stream temperature immediately so that the pump's speeds can be adjusted accordingly. Meanwhile, *Display temperature* is the rendered temperature by the FlexCube, which can be used to evaluate the efficiency of the design and control strategy.

1) Open-loop step transient response: In this experiment, the open-loop transient responses of the temperature system with respect to step input signals are inspected to investigate how fast can the system achieve a target temperature.

Three input values ($input$ = 300, 600, 900) corresponding to three expected stable-state temperatures of 17.1^oC, 26.7^oC, and 37.3^oC respectively (from Fig. 7), are provided to the system. The initial temperature conditions are arbitrary in both the *Mixer* and the FlexCube. The corresponding responses are demonstrated in Fig. 8.

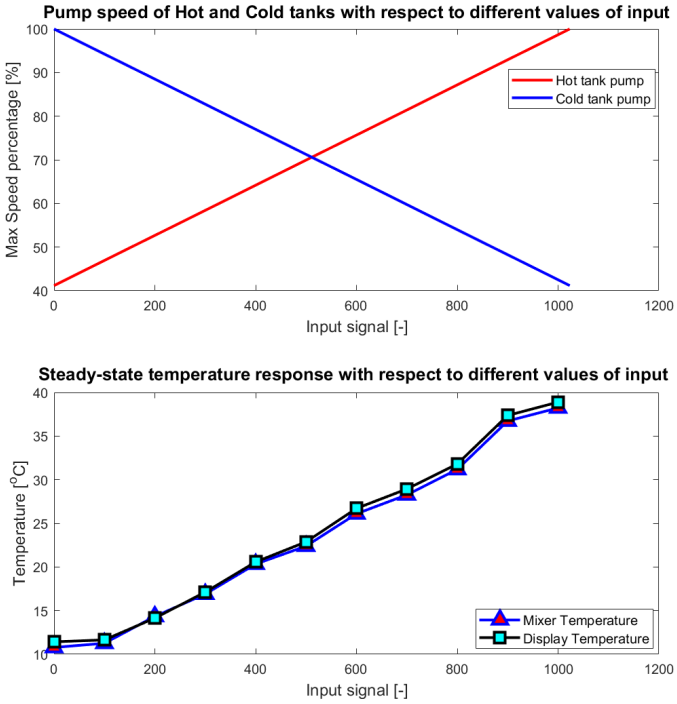

Fig. 7: Variation of pumps' speed (upper) and resulting rendered temperatures (lower) corresponding to different values of $input$ variable

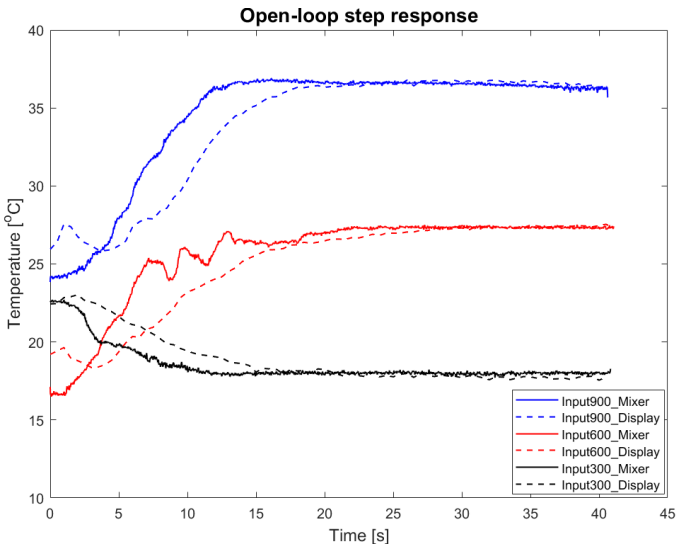

Fig. 8: Open-loop step response for three inputs, 300, 600, and 900.

Firstly, it can be seen that with any given step input signals of $input$, the system shows a similar responding behavior for both *Mixer temperature* and *Display temperature*. In detail, the temperatures slowly approach a steady-state value for different inputs, just like the behavior of a first-order system. Also, the *Display temperatures* always shows a delay effect compared to the *Mixer* response, no matter which input values. The delay time is computed to be approximately 5 seconds for all the inputs. Besides, for each step input value, both the *Mixer* and *Display temperature* eventually converge to the same steady-state value.

The step response characteristics from 3 inputs are shown in Table I. Notably, most of the overshoot and steady-state error values are smaller than 1, which is negligible, except for *Mixer temperature* for $input = 900$. At around the 10 last seconds of the measurement, the steady-state temperatures show a slight decline due to the change of temperatures of the *Hot* and *Cold* tanks after a long running time. Therefore, for future user-study experiments, the stimuli should be limited to a maximum of 15 seconds to ensure the assumption of constant T_{hot} and T_{cold} in Eq. 3.

TABLE I: Open loop response characteristics of temperature rendering system

Input	300		600		900	
	Mixer	Display	Mixer	Display	Mixer	Display
Rise time	6.42	13.3	6.81	13.52	7.18	13.07
Overshoot	0.53	0.32	0.42	0.35	3.78	0.68
SS error	0.12	0.39	0.07	0.08	0.2	0.06

Another special detail is that regardless of the arbitrary initial conditions, the rise time values corresponding to all inputs are comparable for both *Mixer temperature* and *Display temperature* separately. This feature was more closely inspected by a follow-up experiment, where one input ($input = 600$) is provided when the system is at different initial temperatures (both in the FlexCube and the *Mixer*). The corresponding responses with respect to 3 randomly set initial temperatures are demonstrated in Fig. 9. The graphs show that the transient time to approach the (same) steady-state temperature from all 3 different initial conditions is almost similar, which means the initial temperature has little effect on the response time of the system. In other words, no matter what the current temperature is, the time it takes to reach a given temperature is almost unchanged.

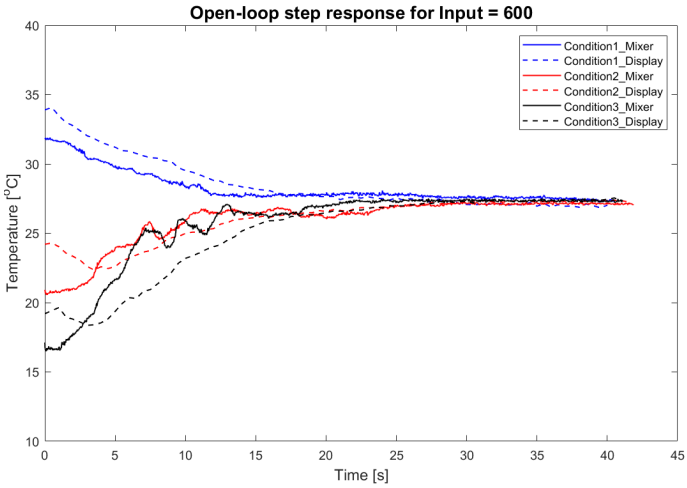

Fig. 9: Open-loop step response for input = 600.

2) Closed-loop step response: Next, a PID controller is designed and applied to control the *Display temperature* to track a given profile. The utilized PID parameters are shown in Appendix [A]. Six constant step profiles (at 15, 20, 25, 30, 35, and 40^oC) are used in the Closed-loop response

experiment. The initial *Display temperature* for all the cases is $25^oC. The resulting responses are depicted in Fig. 10$.

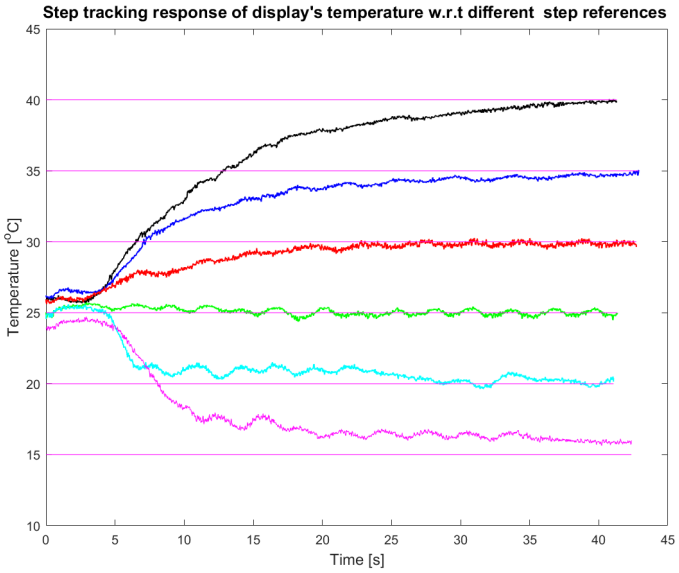

Fig. 10: Step tracking response of display temperature w.r.t different step values

It is noteworthy that the system behavior in Closed-loop (with a PID controller applied) is expected to be different from the Open-loop responses. Overall, the tracking performance is the best for the intermediate temperatures (20, 25, and 30^oC). For high temperatures (35 and 40^oC), although the *Display temperature* can eventually reach the target temperature, the rising time is apparently much longer compared to other cases. On the contrary, the responses corresponding to low-temperature steps (15 and 20^oC) show a quick response tendency with significantly low rising time. However, there always exists considerable steady-state errors in the response of these two scenarios, which makes them unable to reach the target temperature during the entire measuring time ($\approx 40s$).

3) Closed-loop texture profile tracking: When we touch a real texture or material with our finger at room temperature, a heat transfer process will happen in which a heat flux will flow from the finger into that material, leading to temperature changes in both the material and the finger's skin at the contact area. Touching different materials at the same room temperature, however, can give us different thermal sensations, even though all materials have similar temperatures initially. This phenomenon originates from the difference in the heat transfer coefficient of those materials, making the temperature changing rate and temperature steady-state vary among them, and therefore giving us different perceptional information [51].

During the user-study experiment, we want to replicate the thermal sensation that a real material can deliver to the human's finger. In [52], the authors proposed a method referring to the use of heat flux measurement from the user's interaction with real material and then trying to regenerate that heat flux with the haptic display. In specific, the heat flux value at one instant when we touch a material is given as:

$$q = \frac{T_f - T_m}{R} \tag{6}$$

In which q is the heat flux, T_f and T_m are, respectively, the finger's and material's temperatures, and R is the thermal contact resistance. The value of R is unique for each material and surface quality. For samples with smooth surface finishes similar to those produced by my milling, the value of R can be estimated [52] via the thermal conductivity k of the material as follows:

$$R = \frac{0.37 + k}{1870.k} \tag{7}$$

From Eq. 6, if we obtain the heat flux from the real material interaction, we can find out the needed *Display temperature* to regenerate similar values of heat flux, as below:

$$T_d = T_f - q.R \tag{8}$$

where T_d now is the expected *Display temperature*. To inspect the ability to track the T_d profile of the FlexCube, we conduct an experiment by using the data from the SENS3 database [53]. The obtained temperature profile for the Display is shown as the blue continuous line in Fig.11. However, from the information about the system's behavior and response time, it appears that the system can hardly perfectly track a steep curve as we wanted. Therefore, we generated a pseudo profile from the real one by transmitting the curvy trajectory in two steps signal (dashed black line). The pseudo profile consists of two steps: one takes the value of the real profile at $12s$, and one takes the steady-state value of the real profile. The period of $12s$ is selected based on the response in the Closed-loop step response at neutral temperatures, where the rising time of the response is approximately $12s$.

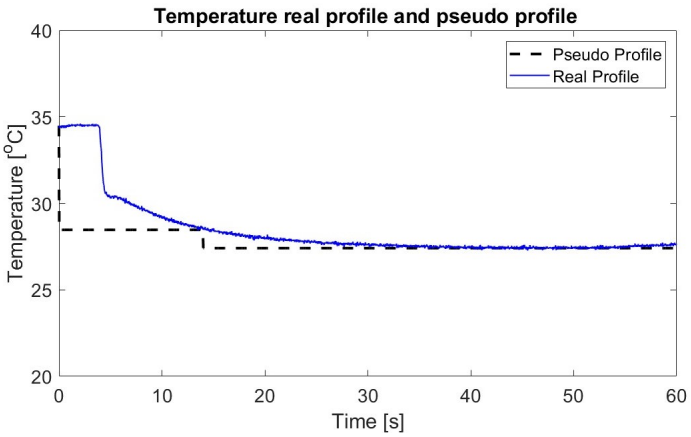

Fig. 11: Temperature real and pseudo profile of the FlexCube.

The tracking results are shown in Fig.12. The pseudo profile appears to be significantly beneficial when the *Display temperature* can replicate the expected curve from the real profile. There is a considerable delay, as predicted. However, this is not a problem for the stimuli rendering work since we can compensate for this delay by instructing the participants to wait for a certain amount of time before starting to interact with the Flexcub. The delayed response, therefore, will not affect the user's perception in the further experiment stage.

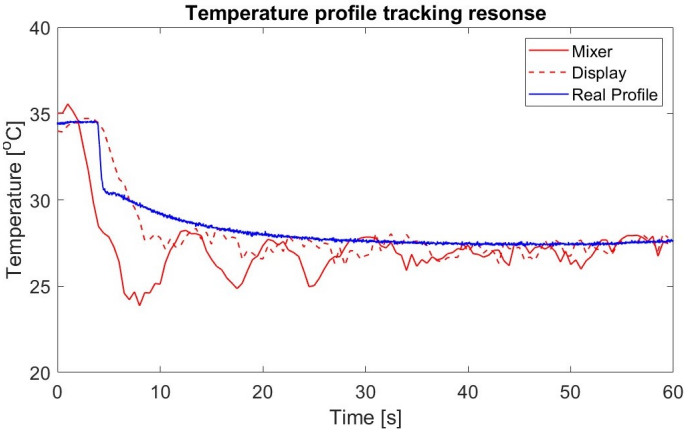

Fig. 12: Display and Mixer temperatures response upon real profile.

B. Contact Area rendering characteristics

As mentioned in Section III, the contact area is controlled via the weight of the amount of water inside the FlexCube. The relations between water weight and contact area with respect to different finger indentation forces are depicted in Fig. 13. During operation, with a given target contact area and the indentation force data received from the FSR sensor, we can always deduce a target water weight inside the FlexCube. The hydraulic system is then modulated to make sure the weight of water inside the FlexCube can reach the aforementioned target weight.

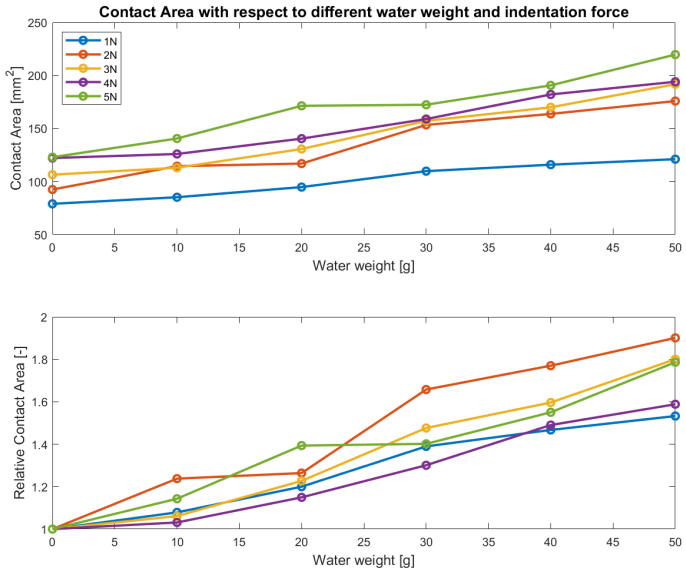

Fig. 13: Relationship between water weight versus absolute (upper) and relative (lower) contact area.

A simple three-state controller is designed for the weight-tracking task, which either accelerates or decelerates the speed of pumps **P3** and **P4** to make sure the current water weight can follow the targeted weight. The pseudo-code of the control algorithm applied can be found in Appendix [A].

The step-tracking experiment was conducted to inspect the behavior and response of the system with this control strategy. A profile of square pulses with $50g$ step height, which is the expected maximum weight of the water inside, and a period of $8s$ is utilized. The resulting response is shown in Fig.14.

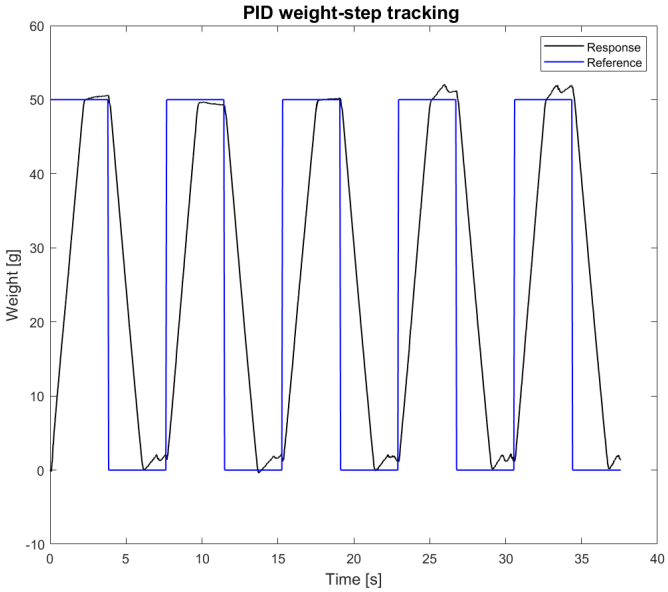

Fig. 14: PID weight-step tracking.

The response characteristics are then averaged between 5 periods. The results showed that the rise time of the system is 2.16s for both step-up and step-down cases. The average steady-state error is approximately $1.8g$, which is 3.6% of the step height. The overshoot can be up to $2g$ at some period and only happens for a step-up scenario. The step-down case, on the other hand, experiences some undershoot due to the elastic force of the foldable 1-DoF origami structure inside.

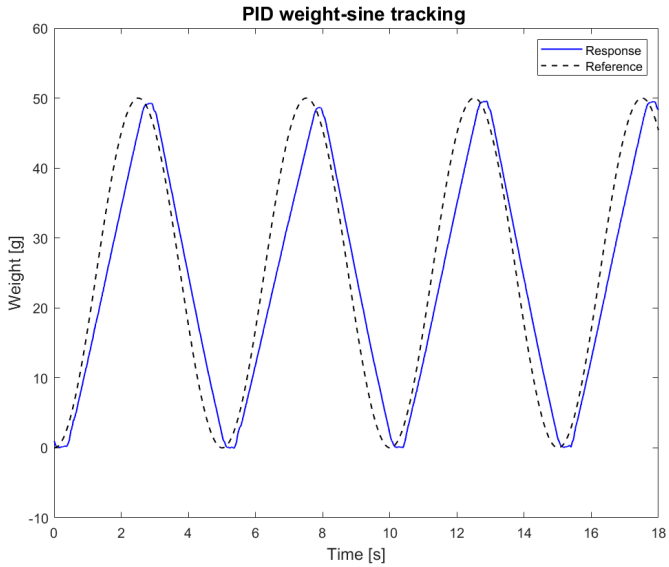

Fig. 15: PID weight-sine tracking.

Since the system can reach 90% of the maximum weight in $2.16s$, it is expected that the contact area rendering system can follow a sinusoidal profile with $5s$ period because it takes $2.5s$ to go from the bottom to the peak of the wave. A sine wave

is interested in this characterization work because its profile is similar to the trajectory of the finger's pushing movement when we explore a soft surface. The sine wave tracking result is shown in Fig. 15. Although there is a phase lag in the response, the maximum delay value, happening mostly at the peak, is only $0.35s$, which can trigger the sensation of viscosity for the user.

C. Roughness rendering characteristics

The efficiency of the electrovibration module is validated by examining the average electrostatic force and friction coefficient that can be generated at one given AC voltage amplitude and frequency. A simple force sensing setup is built for this experiment, as shown in Fig.16. In this experiment, a participant will apply a force of $0.2N$ on the electrovibration film, which is measured by a 6-axis force sensor (Nano43) installed at the bottom of the film, before starting to slide horizontally back and forth with an expected speed of $40mm/s$. The motion of the finger is captured by a motion-tracking sensor (zForce Air) and projected on a monitor placed in front of the user. The sliding speed is maintained by showing an animation of a moving cube with the expected speed and trajectory on the monitor so that the participant can follow the cube's movement to reach the intended speed.

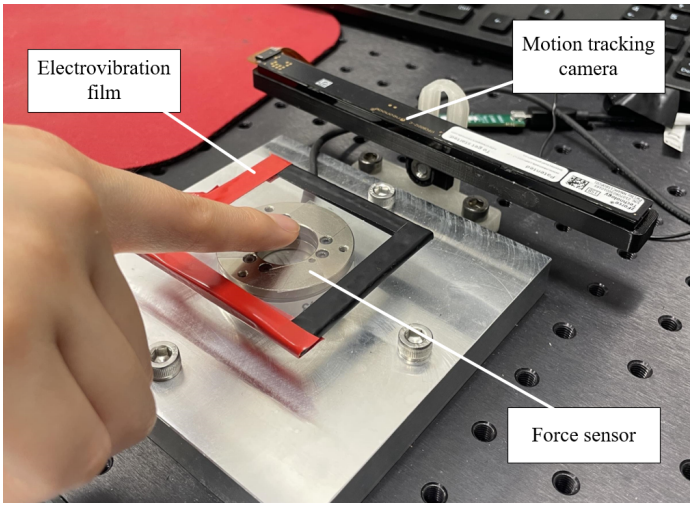

Fig. 16: Experimental force sensing setup.

Four voltage amplitude values ($50Vpp$, $100Vpp$, $150Vpp$, $200Vpp$) and ten frequencies evenly distributed in logarithm scale ranging from $10Hz$ to $1000Hz$ (10 17 28 46 77 129 215 359 599 1000 Hz) are utilized as stimuli for this experiment. The duration of one stimulus is $10s$, and the sampling frequency is $20kHz$. The recorded normal and lateral force values are first low-pass filtered at $1000Hz$ cut-off frequency to remove noise. Each dataset is then divided into 4 segments where the sliding movement is the most stable.
For friction coefficient calculation, in each segment, the lateral force values are divided by the normal force values at the same sample before getting averaged to obtain the friction coefficient of one segment. The achieved results from 4 segments are then averaged one more time to obtain the friction coefficient of one stimulus pattern. The results of this process are shown in Fig. 16.

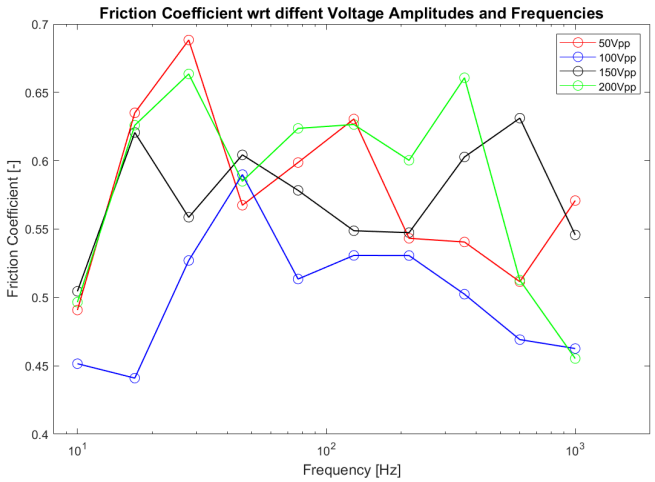

Fig. 17: Friction coefficient w.r.t. various Voltage amplitudes and frequencies.

Generally speaking, the resulting graph shows that the Friction coefficient is proportional to the provided voltage amplitude, which means higher amplitude leads to higher friction sensation. The frequencies, on the other hand, do not show any clear effect on the friction coefficient. The general trend appears to be an increase of friction at first, followed by a wide flat region with nearly equal values, before going down again after $300Hz$.

For measuring the Electrovibration force generated by the electrovibration film, a bandpass filter is utilized and applied at the frequency that the force appears. Since the electrovibration force's frequency is two times the applied voltage frequency, we need to apply the bandpass filter with the cut-off frequency range of $(2f_V \pm 5Hz)$ for the voltage frequencies of $f_V = 10, 17, 28, 46, 77Hz$, and the range of $(2f_V \pm 10Hz)$ for the remaining voltage frequencies. After that, for each of the segmented datasets, the root-mean-square (RMS) of the lateral and normal force are determined. The amplitude of the forces is then calculated by multiplying the RMS values with $\sqrt{2}$, before summing up the amplitude values from the lateral and the normal force to obtain the total amplitude of Electrovibration force of one segment. The amplitude values from 4 segments are finally averaged to achieve the Electrovibration force amplitude at one given stimulus. The results are demonstrated in Fig. 18.

The resulting graph verifies the conclusion drawn from the previous graph: the higher the applied voltage, the higher the electrovibration force (and, therefore the friction coefficient) at every examined frequency. Moreover, the plots of $150Vpp$ and $200Vpp$ show two peaks at the same frequencies: $17Hz$ and $599Hz$, while the plots of $150Vpp$ and $200Vpp$ hardly show any unusual variation. Especially all 4 plots corresponding to 4 voltage amplitudes show a significant drop in electrovibration force amplitude at 1000 Hz, which can be explained by the usage of the low-pass filter with the cut-off frequency at 1000 Hz as well.

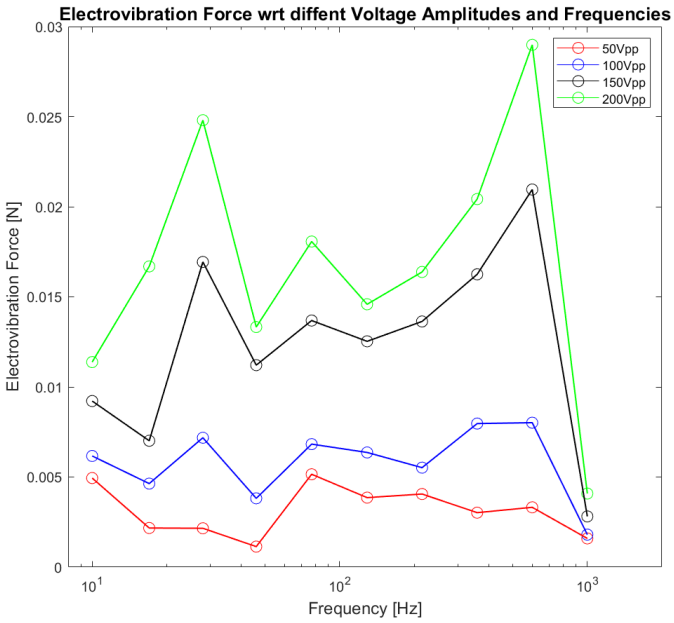

Fig. 18: Electroviberation force w.r.t. different voltages and frequencies.

To validate the Electrovibration force results obtained from the experiment, an analytical calculation was made to give a quick comparison in the ideal scenario. From [54], the electrovibration force acting on the stratum corneum of our finger is calculated as:

$$F_e = \frac{\varepsilon_0 \varepsilon_{SC}}{2} \left(\frac{V_{SC}}{d_{SC}} \right)^2 \tag{9}$$

where ε_0 is the permittivity of vacuum, ε_{SC} is the relative permittivity of the stratum corneum, A the area of the fingertip when in contact, d_{SC} is the thickness of the stratum corneum and V_{SC} is the voltage across the stratum corneum. The value of V_{SC} is related to the voltage applied to the whole film by the formula:

$$V_{SC} = V \frac{Z_{SC}}{Z_{SC} + Z_{body} + Z_{insulator}} \tag{10}$$

in which Z_{body}, Z_{SC}, and $Z_{insulator}$ are the impedances of the human body, stratum corneum, and the electrovibration's insulator layer, respectively. Using the empirical parameters relating to the stratum corneum and the body in [54], the resulting theoretical electrovibration forces are achieved as below:

TABLE II: Analytical calculation of Electrovibration force with amplitude of 200 Vpp

Frequency	Force (N)	Frequency	Force (N)
10	0.0001	129	0.0037
17	0.0003	215	0.0044
28	0.0006	359	0.0047
46	0.0014	599	0.0048
77	0.0026	1000	0.0049

The resulting forces from analytical calculations seem to be 10 times smaller than those measured in the experiment. The reason may come from the uncertainty of the insulator (Resin) dielectric constant since this property can be changed when we mix it with a thinner solution (Acetone).

Besides, a COMSOL model was built with 3 objects: ITO layer, Resin layer, and Stratum corneum with similar dimensions utilized in the previous analytical calculation Fig. 19. The forces obtained from the simulation appear to be unaffected by frequency and maintained at a constant value of $0.0103N$, which is more comparable to the results from the experiment. In general, further work will need to be done to find out a decent explanation for these differences.

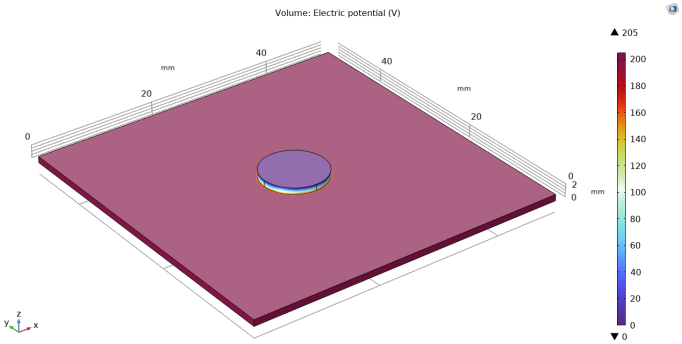

Fig. 19: FEM simulation - Electrical potential voltage distribution of a stationary simulation.

V. Discussion

A. For hydraulic module

In general, the hydraulic system has been proven to be capable of delivering the desired value, for both temperature and contact area (in the form of weight) aspects.

This hydraulic-based temperature rendering system, from a modeling perspective, has an infinite number of stable states since the *Display temperature* will remain unchanged when we stop giving the input signal. This property is beneficial when we can maintain the temperature inside the FlexCube without providing any further energy (at a short time when heat emission can be neglected), which theoretically can save us a lot of time from waiting for the temperature to rise again whenever the system is switched off.

However, as pointed out in the Open-loop step response experiment, the *Display temperature* rising time is not affected by the initial temperature condition of the water stored inside the FlexCube. The reason is that, different from other temperature rendering interfaces (such as Peltier element) which need time to either heat up or cool down a physical object, the hydraulic-based system does not really change the temperature of any object because as the flow keeps on flowing, the old volume of water will flow out and the new volume of water with different temperatures can appear immediately without the need for continuity in the temperature of the flow. For example, when a mixed streamline is flowing normally with the operation of both pumps, pump P1 suddenly stops (giving no more flow of hot water), and pump P2 runs at full speed, an amount of 10^oC water will suddenly appear right behind the previous mixed streamline, creating a flow with two significantly different local temperature.

Besides, up to now, we are solely looking into the measurement of the water temperature inside the FlexCube, not on its top surface. When the user touches the FlexCube, they will perceive the temperature of the top surface, not the water below. Since the top surface is a physical object, the delay phenomenon due to heat transfer will occur. Therefore, it is necessary to examine the surface's temperature during the stimulation process to verify the effectiveness of the temperature rendering work.

For the contact area rendering task, the hydraulic system appears to well perform in the weight-tracking task with a low response time and steady-state error. However, the most challenging part of this mechanism is to relate the finger contact area with the real volume of water needed to be filled inside the FlexCube. The problem is that this relationship depends on the geometry of the finger. In specific, from a certain finger indentation distance performed by the user, we can come up with a value of the contact area that we want to deliver accordingly. However, when we transfer from the desired contact area to the corresponding desired water volume inside the FlexCube, the size and shape of the finger really matter and significantly affect the calculation of the target water volume. Currently, we can partly mitigate this issue by recording the *contact area - water volume relationship* curve of many participants before averaging them to obtain the most meaningful and suitable curve for this contact area controlling task.

B. For Roughness Module

Overall, this module has shown good performance when the roughness sensations delivered are vivid and perceptible for most of the frequencies in the inspected range. The fact that it can stimulate such a salient sensation is especially important when integrated into a multimodal device since the user can easily get distracted or overwhelmed by other tactile modalities if the rendered stimuli are too subtle. The only problem with this module is the non-uniformity of the coating thickness, which will moderately affect the user's perception during the experiment if they accidentally move their fingers too far to the corner. The origin of this issue lies in the nature of the spin-coating process when the coating substance is distributed by centrifugal force, which always results in a thicker coating in the center and gradually thinner when moving away from the center.

Besides, since this electrovibration film is flexible, the coating thickness can also be changed when the film deforms due to the finger's indenting movement. However, the change in the coated film's capacitance is shown to be insignificant with respect to different radii of curvature [Appendix C]. As capacitance is inversely proportional to thickness, this result can more or less ensure that the perceived roughness will hardly be affected by the deformation of the FlexCube's top surface.

Moreover, the measurement of electrovibration force is conducted in a certain constrained condition, with 0.2N pushing force and 40 mm/s sliding speed, which were adjusted and maintained by the use of the force sensor and the motion tracking sensor, respectively. Meanwhile, during a real human experiment, it is much more challenging to make sure the user can perform any desired conditions. And since the conditions are not ensured anymore, the resulting roughness perception is unpredictable. Therefore, further characteristic experiments need to be done with different conditions so that we can have a more reliable estimation of the perceived roughness by the users in the free exploration movement.

C. Future Work

In the next phase of the research, we will conduct a user-study experiment to investigate the subjective tactile sensation that the FlexCube can deliver. The temperature profiles of more materials will be used to provide a wider range of variation in thermal cues. For the electrovibration module, the possibly generated sensations are roughness, bumpiness, and stickiness. One possible next step is to conduct a threshold experiment to find out the perceptional limit of humans when interacting with our device. Based on the data of the threshold and the obtained resulting forces, the most salient sets of stimuli will be selected to ensure providing vivid and perceptible sensations. During the experiment, the participants will give answers regarding the levels of the sensations they perceive with a set of adjective scales. The achieved data will then be analyzed to find out the principle dimensions of the perceptual space of FlexCube. Also, those data help us find out the relation between one sensation and other physical quantities used to deliver the stimuli.

In conclusion, the FlexCube has shown good potential to become a distinctive flexible haptic interface with deformability properties and the capability of delivering 3 tactile sensations. This device can be applied in the field of E-commerce with the ability to stimulate the virtual texture and touch sensation of any given product. When the customers want to inspect a piece of cloth with a bare finger at a long distance, they can touch and interact with the FlexCube instead and still get the idea of how soft, smooth, or warm the real cloth is.

REFERENCES

[1] J. Qi, F. Gao, G. Sun, J. C. Yeo, and C. T. Lim, "Haptglove—untethered pneumatic glove for multimode haptic feedback in reality–virtuality continuum," *Advanced Science*, vol. 10, no. 25, p. 2 301 044, 2023. DOI: https://doi.org/10.1002/advs.202301044. eprint: https://onlinelibrary.wiley.com/doi/pdf/10.1002/advs.202301044. [Online]. Available: https://onlinelibrary.wiley.com/doi/abs/10.1002/advs.202301044.

[2] X. Gu, Y. Zhang, W. Sun, Y. Bian, D. Zhou, and P. O. Kristensson, "Dexmo: An inexpensive and lightweight mechanical exoskeleton for motion capture and force feedback in vr," in *Proceedings of the 2016 CHI Conference on Human Factors in Computing Systems*, ser. CHI '16, San Jose, California, USA: Association for Computing Machinery, 2016, pp. 1991–1995, ISBN: 9781450333627. DOI: 10.1145/2858036.2858487. [Online]. Available: https://doi.org/10.1145/2858036.2858487.

[3] J. Heredia, J. Tirado, V. Panov, M. A. Cabrera, K. Youcef-Toumi, and D. Tsetserukou, "Recyglide: A forearm-worn multi-modal haptic display aimed to improve user vr immersion submission," in *Proceedings of the 25th ACM Symposium on Virtual Reality Software and Technology*, ser. VRST '19, Parramatta, NSW, Australia: Association for Computing Machinery, 2019, ISBN: 9781450370011. DOI: 10.1145/3359996.3364759. [Online]. Available: https://doi-org.tudelft.idm.oclc.org/10.1145/3359996.3364759.

[4] Y. Huang, J. Zhou, P. Ke, *et al.*, "A skin-integrated multimodal haptic interface for immersive tactile feedback," *Nature Electronics*, vol. 6, pp. 1–12, Nov. 2023. DOI: 10.1038/s41928-023-01074-z.

[5] A. Talhan, H. Kim, and S. Jeon, "Tactile ring: Multimode finger-worn soft actuator for rich haptic feedback," *IEEE Access*, vol. 8, pp. 957–966, 2020. [Online]. Available: https://api.semanticscholar.org/CorpusID:209900921.

[6] H. A. J. van Riessen and Y. Vardar, *Relocating thermal stimuli to the proximal phalanx may not affect vibrotactile sensitivity on the fingertip*, 2023. arXiv: 2312.07261 [cs.HC]. [Online]. Available: https://arxiv.org/abs/2312.07261.

[7] B. L. Kodak and Y. Vardar, "Feelpen: A haptic stylus displaying multimodal texture feels on touchscreens," *IEEE/ASME Transactions on Mechatronics*, vol. 28, no. 5, pp. 2930–2940, 2023. DOI: 10.1109/TMECH.2023.3264787.

[8] A. Arasan, C. Basdogan, and T. M. Sezgin, "Haptic stylus with inertial and vibro-tactile feedback," in *2013 World Haptics Conference (WHC)*, 2013, pp. 425–430. DOI: 10.1109/WHC.2013.6548446.

[9] J. C. Lee, P. H. Dietz, D. Leigh, W. S. Yerazunis, and S. E. Hudson, "Haptic pen: A tactile feedback stylus for touch screens," in *Proceedings of the 17th Annual ACM Symposium on User Interface Software and Technology*, ser. UIST '04, Santa Fe, NM, USA: Association for Computing Machinery, 2004, pp. 291–294, ISBN: 1581139578. DOI: 10.1145/1029632.1029682. [Online]. Available: https://doi.org/10.1145/1029632.1029682.

[10] G. Kim, D. Hwang, and J. Park, "Effect of 2.5d haptic feedback on virtual object perception via a stylus," *Scientific Reports*, vol. 11, no. 1, p. 18954, Sep. 2021, ISSN: 2045-2322. DOI: 10.1038/s41598-021-98589-2. [Online]. Available: https://doi.org/10.1038/s41598-021-98589-2.

[11] W. Hassan, H. Kim, A. Talhan, and S. Jeon, "A pneumatically-actuated mouse for delivering multimodal haptic feedback," *Applied Sciences*, vol. 10, no. 16, 2020, ISSN: 2076-3417. DOI: 10.3390/app10165611. [Online]. Available: https://www.mdpi.com/2076-3417/10/16/5611.

[12] W. Park, S. Park, L. Kim, and S. Shin, "Haptic mouse interface actuated by an electromagnet," in *2011 International Conference on Complex, Intelligent, and Software Intensive Systems*, 2011, pp. 643–646. DOI: 10.1109/CISIS.2011.107.

[13] I. Kumazawa, "Haptic mouse with quick and flexible tactile feedback generated by double control loop," in *19th International Symposium in Robot and Human Interactive Communication*, 2010, pp. 664–669. DOI: 10.1109/ROMAN.2010.5598712.

[14] M. İ. C. Dede, Ö. Selvi, T. Bilgincan, and Y. Kant, "Design of a haptic device for teleoperation and virtual reality systems," in *2009 IEEE International Conference on Systems, Man and Cybernetics*, 2009, pp. 3623–3628. DOI: 10.1109/ICSMC.2009.5346857.

[15] D. Dhivin, J. Jose, and R. R. Bhavani, "Bilateral telehaptic interface for controlling a robotic manipulator," in *2017 International Conference on Intelligent Computing, Instrumentation and Control Technologies (ICICICT)*, 2017, pp. 1614–1620. DOI: 10.1109/ICICICT1.2017.8342812.

[16] P. Lambert and J. L. Herder, "A 7-dof redundantly actuated parallel haptic device combining 6-dof manipulation and 1-dof grasping," *Mechanism and Machine Theory*, vol. 134, pp. 349–364, 2019, ISSN: 0094-114X. DOI: https://doi.org/10.1016/j.mechmachtheory.2019.01.002. [Online]. Available: https://www.sciencedirect.com/science/article/pii/S0094114X18316513.

[17] M. Nakatani, K. Sato, K. Sato, *et al.*, "A novel multimodal tactile module that can provide vibro-thermal feedback," in *Haptic Interaction*, S. Hasegawa, M. Konyo, K.-U. Kyung, T. Nojima, and H. Kajimoto, Eds., Singapore: Springer Singapore, 2018, pp. 437–443, ISBN: 978-981-10-4157-0.

[18] S. Gallo, C. Son, H. J. Lee, H. Bleuler, and I.-J. Cho, "A flexible multimodal tactile display for delivering shape and material information," *Sensors and Actuators A: Physical*, vol. 236, pp. 180–189, 2015, ISSN: 0924-4247. DOI: https://doi.org/10.1016/j.sna.2015.10.048. [Online]. Available: https://www.sciencedirect.com/science/article/pii/S0924424715302090.

[19] J.-U. Lee, J.-M. Lim, H. Shin, and K.-U. Kyung, "A haptic touchscreen interface for mobile devices," in *Proceedings of the 15th ACM on International Conference on Multimodal Interaction*, ser. ICMI '13, Sydney, Australia: Association for Computing Machinery, 2013, pp. 311–312, ISBN: 9781450321297. DOI: 10.1145/2522848.2531757. [Online]. Available: https://doi-org.tudelft.idm.oclc.org/10.1145/2522848.2531757.

[20] R. Ilhan and T. Allahverdiyev, "Multimodal soft tactile display," in *2021 5th International Symposium on Multidisciplinary Studies and Innovative Technologies (ISMSIT)*, 2021, pp. 660–663. DOI: 10.1109/ISMSIT52890.2021.9604759.

[21] M. Hollins, R. Faldowski, S. Rao, and F. Young, "Perceptual dimensions of tactile surface texture: A multidimensional scaling analysis," *Perception psychophysics*, vol. 54, pp. 697–705, Jan. 1994.

[22] M. Hollins, S. Bensmaia, K. Karlof, and F. Young, "Individual differences in perceptual space for tactile textures: Evidence from multidimensional scaling," *Perception and Psychophysics*, vol. 62, pp. 1534–1544, Apr. 2012. DOI: 10.3758/BF03212154.

[23] R. Roberts, A. Loomes, H. Allen, M. Di Luca, and A. Wing, "Contact forces in roughness discrimination," *Scientific Reports*, vol. 10, Mar. 2020. DOI: 10.1038/s41598-020-61943-x.

[24] D. Katz, "Der aufbau der tastwelt," *Annalen der Philosophie Und Philosophischen Kritik*, vol. 5, no. 5, pp. 150–151, 1925.

[25] A. T. Maereg, A. Nagar, D. Reid, and E. L. Secco, "Wearable vibrotactile haptic device for stiffness discrimination during virtual interactions," *Frontiers in Robotics and AI*, vol. 4, 2017, ISSN: 2296-9144. DOI: 10.3389/frobt.2017.00042. [Online]. Available: https://www.frontiersin.org/journals/robotics-and-ai/articles/10.3389/frobt.2017.00042.

[26] P. Strohmeier and K. Hornbæk, "Generating haptic textures with a vibrotactile actuator," in *Proceedings of the 2017 CHI Conference on Human Factors in Computing Systems*, ser. CHI '17, Denver, Colorado, USA: Association for Computing Machinery, 2017, pp. 4994–5005, ISBN: 9781450346559. DOI: 10.1145/3025453.3025812. [Online]. Available: https://doi.org/10.1145/3025453.3025812.

[27] R. Ilhan and K. Kaçanoğlu, "Tactile feedback on a fabric surface using electrovibration," in *2021 3rd International Congress on Human-Computer Interaction, Optimization and Robotic Applications (HORA)*, 2021, pp. 1–4. DOI: 10.1109/HORA52670.2021.9461341.

[28] H. Ishizuka, K. Suzuki, K. Terao, H. Takao, F. Shimokawa, and H. Kajimoto, "Development of a multi-electrode electrovibration tactile display with 1 mm resolution," in *2017 IEEE World Haptics Conference (WHC)*, 2017, pp. 659–664. DOI: 10.1109/WHC.2017.7989979.

[29] H. Ishizuka, R. Hatada, C. Cortes, and N. Miki, "Development of a fully flexible sheet-type tactile display based on electrovibration stimulus," *Micromachines*, vol. 9, no. 5, 2018, ISSN: 2072-666X. DOI: 10.3390/mi9050230. [Online]. Available: https://www.mdpi.com/2072-666X/9/5/230.

[30] C. D. Shultz, M. A. Peshkin, and J. E. Colgate, "Surface haptics via electroadhesion: Expanding electrovibration with johnsen and rahbek," *2015 IEEE World Haptics Conference (WHC)*, pp. 57–62, 2015. [Online]. Available: https://api.semanticscholar.org/CorpusID:6452221.

[31] Y. Ujitoko, T. Taniguchi, S. Sakurai, and K. Hirota, "Development of finger-mounted high-density pin-array haptic display," *IEEE Access*, vol. 8, pp. 145 107–145 114, 2020. DOI: 10.1109/ACCESS.2020.3015058.

[32] H. Sawada, "Tactile display using the micro-vibration of shape-memory alloy wires and its application to tactile interaction systems," in Apr. 2016, pp. 57–77, ISBN: 978-4-431-55771-5. DOI: 10.1007/978-4-431-55772-2_4.

[33] T.-H. Yang, S.-Y. Kim, C. H. Kim, D.-S. Kwon, and W. J. Book, "Development of a miniature pin-array tactile module using elastic and electromagnetic force for mobile devices," *World Haptics 2009 - Third Joint EuroHaptics conference and Symposium on Haptic Interfaces for Virtual Environment and Teleoperator Systems*, pp. 13–17, 2009. [Online]. Available: https://api.semanticscholar.org/CorpusID:20060165.

[34] D. Prattichizzo, C. Pacchierotti, and G. Rosati, "Cutaneous force feedback as a sensory subtraction technique in haptics," *IEEE Trans Haptics November*, vol. 5, Aug. 2011. DOI: 10.1109/TOH.2012.15.

[35] M. Mete, H. Jeong, W. D. Wang, and J. Paik, "Sori: A softness-rendering interface to unravel the nature of softness perception," *Proceedings of the National Academy of Sciences*, vol. 121, no. 13, e2314901121, 2024. DOI: 10.1073/pnas.2314901121. eprint: https://www.pnas.org/doi/pdf/10.1073/pnas.2314901121. [Online]. Available: https://www.pnas.org/doi/abs/10.1073/pnas.2314901121.

[36] V. Vechev, J. Zarate, D. Lindlbauer, R. Hinchet, H. Shea, and O. Hilliges, "Tactiles: Dual-mode low-power electromagnetic actuators for rendering continuous contact and spatial haptic patterns in vr," Mar. 2019, pp. 312–320. DOI: 10.1109/VR.2019.8797921.

[37] Y. Jung and J. Ramos, "A large force haptic interface with modular linear actuators," *Actuators*, vol. 12, no. 7, 2023, ISSN: 2076-0825. DOI: 10.3390/act12070293. [Online]. Available: https://www.mdpi.com/2076-0825/12/7/293.

[38] P. Olsson, S. Johansson, F. Nysjö, and I. Carlbom, "Rendering stiffness with a prototype haptic glove actuated by an integrated piezoelectric motor," in *Haptics: Perception, Devices, Mobility, and Communication*, P. Isokoski and J. Springare, Eds., Berlin, Heidelberg: Springer Berlin Heidelberg, 2012, pp. 361–372, ISBN: 978-3-642-31401-8.

[39] X. Ke, J. Jiang, Z. Chai, *et al.*, "Stiffness preprogrammable soft bending pneumatic actuators for high-efficient, conformal operation," *Soft robotics*, vol. 9, Jul. 2021. DOI: 10.1089/soro.2020.0207.

[40] A. Stanley, J. Gwilliam, and A. Okamura, "Haptic jamming: A deformable geometry, variable stiffness tactile display using pneumatics and particle jamming," Apr. 2013, pp. 25–30, ISBN: 978-1-4799-0087-9. DOI: 10.1109/WHC.2013.6548379.

[41] B. Li, A. R. Sharpe, and G. J. Gerling, "A transparent hydraulic actuator to visualize finger pad deformation at programmable material compliances," in *2024 IEEE Haptics Symposium (HAPTICS)*, 2024, pp. 61–66. DOI: 10.1109/HAPTICS59260.2024.10520859.

[42] V. E. Hribar and D. T. V. Pawluk, "A tactile-thermal display for haptic exploration of virtual paintings," *The proceedings of the 13th international ACM SIGACCESS conference on Computers and accessibility*, 2011. [Online]. Available: https://api.semanticscholar.org/CorpusID:353525.

[43] L. Peters, G. Serhat, and Y. Vardar, "Thermosurf: Thermal display technology for dynamic and multi-finger interactions," *IEEE Access*, vol. 11, pp. 12 004–12 014, 2023. DOI: 10.1109/ACCESS.2023.3242040.

[44] S. Gallo, G. Rognini, L. Santos-Carreras, T. Vouga, O. Blanke, and H. Bleuler, "Encoded and crossmodal thermal stimulation through a fingertip-sized haptic display," *Frontiers in Robotics and AI*, vol. 2, Oct. 2015. DOI: 10.3389/frobt.2015.00025.

[45] X. Guo, Y. Zhang, W. Wei, W. Xu, and D. Wang, "Thermaltex: A two-modal tactile display for delivering surface texture and thermal information," in *Haptics: Science, Technology, Applications*, I. Nisky, J. Hartcher-O'Brien, M. Wiertlewski, and J. Smeets, Eds., Cham: Springer International Publishing, 2020, pp. 288–296, ISBN: 978-3-030-58147-3.

[46] M. Sakaguchi, K. Imai, and K. Hayakawa, "Development of high-speed thermal display using water flow," vol. 8521, Jun. 2014, pp. 233–240, ISBN: 978-3-319-07730-7. DOI: 10.1007/978-3-319-07731-4_24.

[47] Y. Osawa, Y. Kinbara, M. Kageoka, K. Iida, and A. Kheddar, "Soft robotic shell with active thermal display," *Scientific Reports*, vol. 11, no. 1, p. 20 070, Oct. 2021, ISSN: 2045-2322. DOI: 10.1038/s41598-021-99117-y. [Online]. Available: https://doi.org/10.1038/s41598-021-99117-y.

[48] B. N. J. Persson, "General theory of electroadhesion," *Journal of Physics: Condensed Matter*, vol. 33, no. 43, p. 435 001, Aug. 2021. DOI: 10.1088/1361-648X/abe797. [Online]. Available: https://dx.doi.org/10.1088/1361-648X/abe797.

[49] E. Vezzoli, M. Amberg, G. Frédéric, and B. Lemaire-Semail, "Electrovibration modeling analysis," Jun. 2014, ISBN: 978-3-662-44195-4. DOI: 10.1007/978-3-662-44196-1_45.

[50] J. Jiao, D. Wang, Y. Zhang, *et al.*, "Detection and discrimination thresholds for haptic gratings on electrostatic tactile displays," *IEEE Transactions on Haptics*, vol. PP, pp. 1–1, Jul. 2018. DOI: 10.1109/TOH.2018.2859967.

[51] H.-N. Ho and L. A. Jones, "Contribution of thermal cues to material discrimination and localization," *Perception & Psychophysics*, vol. 68, no. 1, pp. 118–128, Jan. 2006, ISSN: 1532-5962. DOI: 10.3758/BF03193662. [Online]. Available: https://doi.org/10.3758/BF03193662.

[52] L. A. Jones and H.-N. Ho, "Warm or cool, large or small? the challenge of thermal displays," *IEEE Transactions on Haptics*, vol. 1, no. 1, pp. 53–70, 2008. DOI: 10.1109/TOH.2008.2.

[53] J. Kb, B. Kodak, and Y. Vardar, "Sens3: Multisensory database of finger-surface interactions and corresponding sensations," Jul. 2024.

[54] Y. Vardar, B. Güçlü, and C. Basdogan, "Effect of waveform on tactile perception by electrovibration displayed on touch screens," *IEEE Transactions on Haptics*, vol. 10, no. 4, pp. 488–499, 2017. DOI: 10.1109/TOH.2017.2704603.

A

Control algorithm

(K_p), Integral (K_I) and Derivative (K_D) for temperature control

PID parameters for Temperature control

$\mathbf{K_P}$	$\mathbf{K_I}$	$\mathbf{K_D}$
38	7	10

Table A.1: PID parameters

Pseudo-code of Weight control algorithm

```
    if ((weight_error < 0)&&(abs(weight_error) > 3)){
        pump3(pump3_IN1, 255);
        pump3(pump4_IN1, 100);
    }
    else if ((weight_error > 0)&&(abs(weight_error) > 3)){
        pump3(pump3_IN1, 100);
        pump3(pump4_IN1, 255);    }
    else {
        pump3(pump3_IN1, 100);
        pump3(pump4_IN1, 100);
    }
```

B

Coating Recipe

Material properties

The Material	**Young modulus**	**Conductivity**	**Possion's ratio**
ITO	116 GPa	10^6 S/m	0.35
Epoxy Resin	3100 MPa	10^{-8} S/m	0.4
Skin	5 kPa - 140 MPa	$1.42 * 10^{-5}$ S/m	0.48

Spin Coating Recipe for Epoxy Resin on ITO Glass

Materials needed:

- **Substrate: ITO-coated glass slides**
- **Epoxy Resin.**
- **Solvent:** Acetone.
- **Mixing Ratio:** 1:1 (Epoxy Resin)
- **Spin Coater:** With a speed of 3000 RPM.
- **UV Light source:** For curing the resin

Procedure:

First, start by cleaning the ITO glass with Isopropanol solution and mixing the epoxy resin with the acetone in a 1:1 volume ratio. Then secure the cleaned ITO glass substrate onto the spin coater chuck double-sided tape. Set the acceleration to 1000rpm^2, speed to 3000$rpmr$, and duration to 30s. After finishing all the setup, drop the resin solution with a pipette or syringe at the center of the ITO film. Finally, click start the spin-coater. When the sample is done, cure it using a UV light for 3 minutes or more to ensure it is fully cured. Clean the cured sample one more time with Isopropanol before proceeding to any later measurements.

C

Capacitance variation of Epoxy Resin

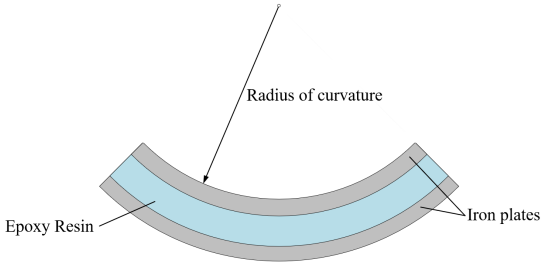

Figure C.1: Setup for measuring capacitance of Epoxy Resin layer.

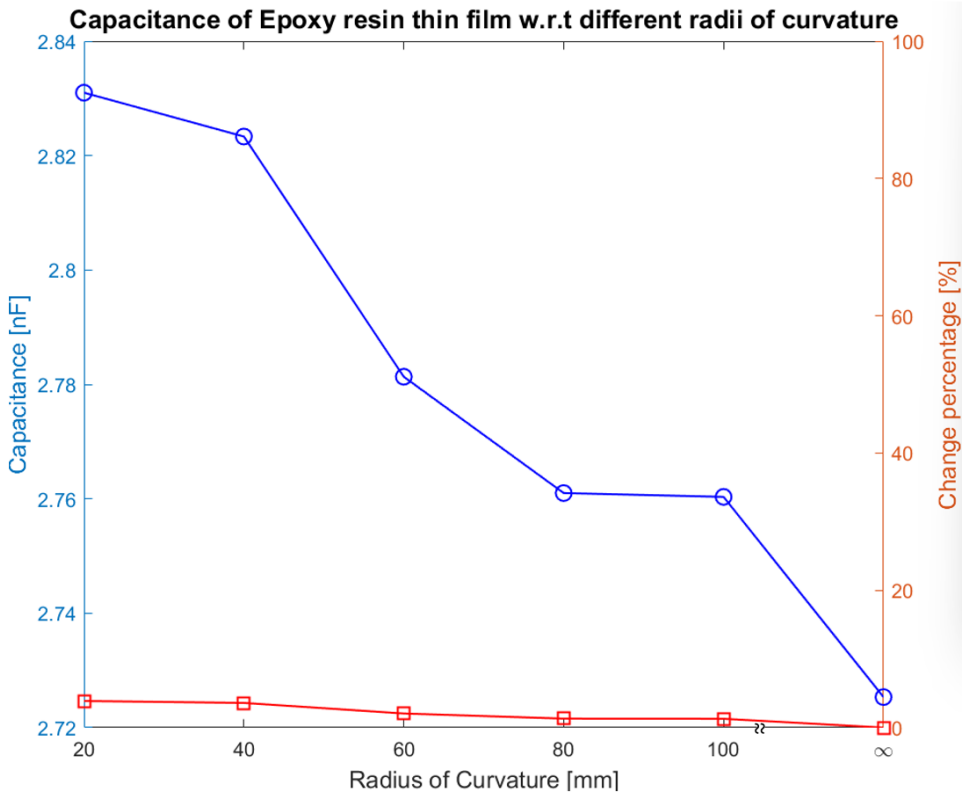

Figure C.2: Variation of Epoxy Resin's Capacitance (relative and absolute) w.r.t. radii of curvature

D

Thickness measurements of Epoxy Resin layer

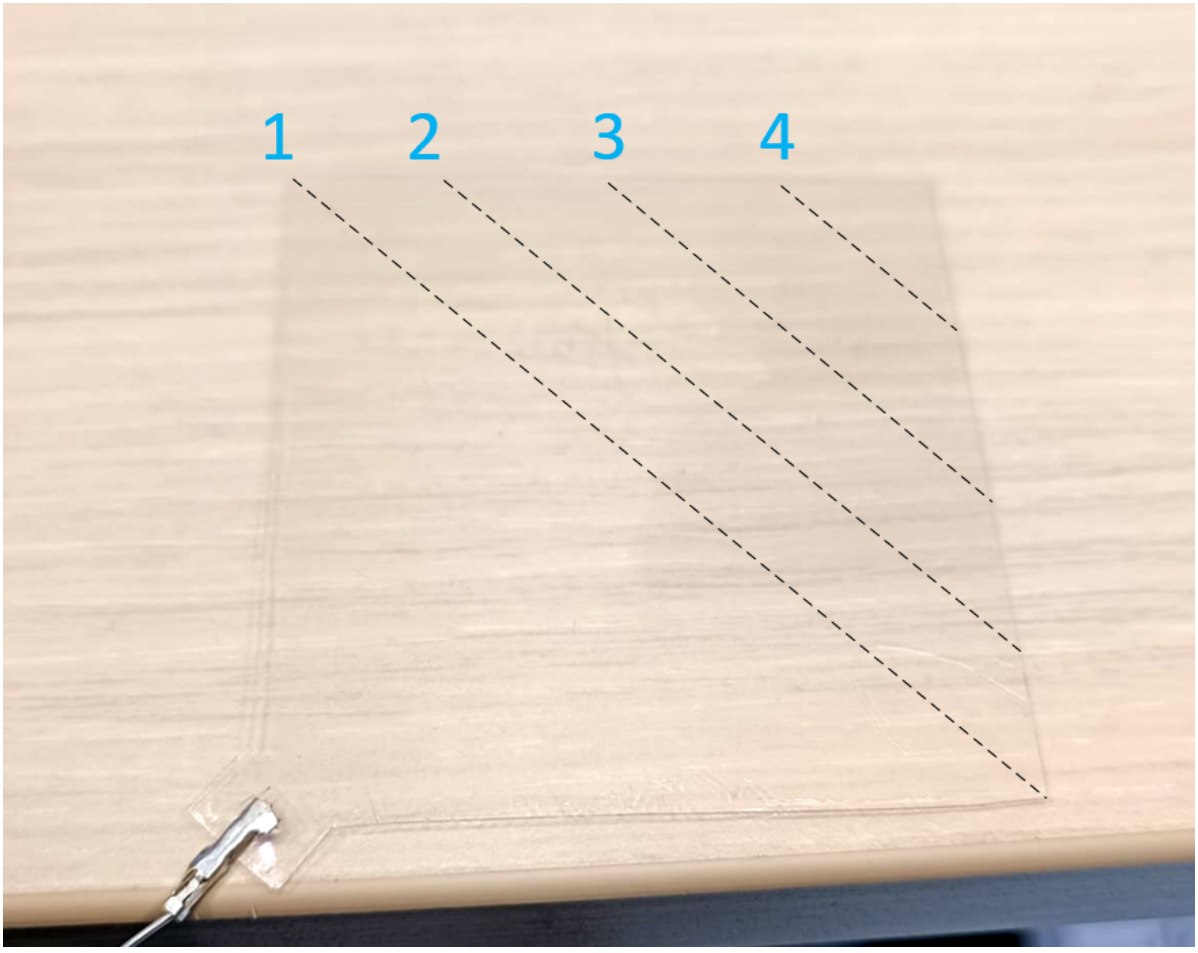

Figure D.1: 4 inspection lines utilized to measure coating thickness

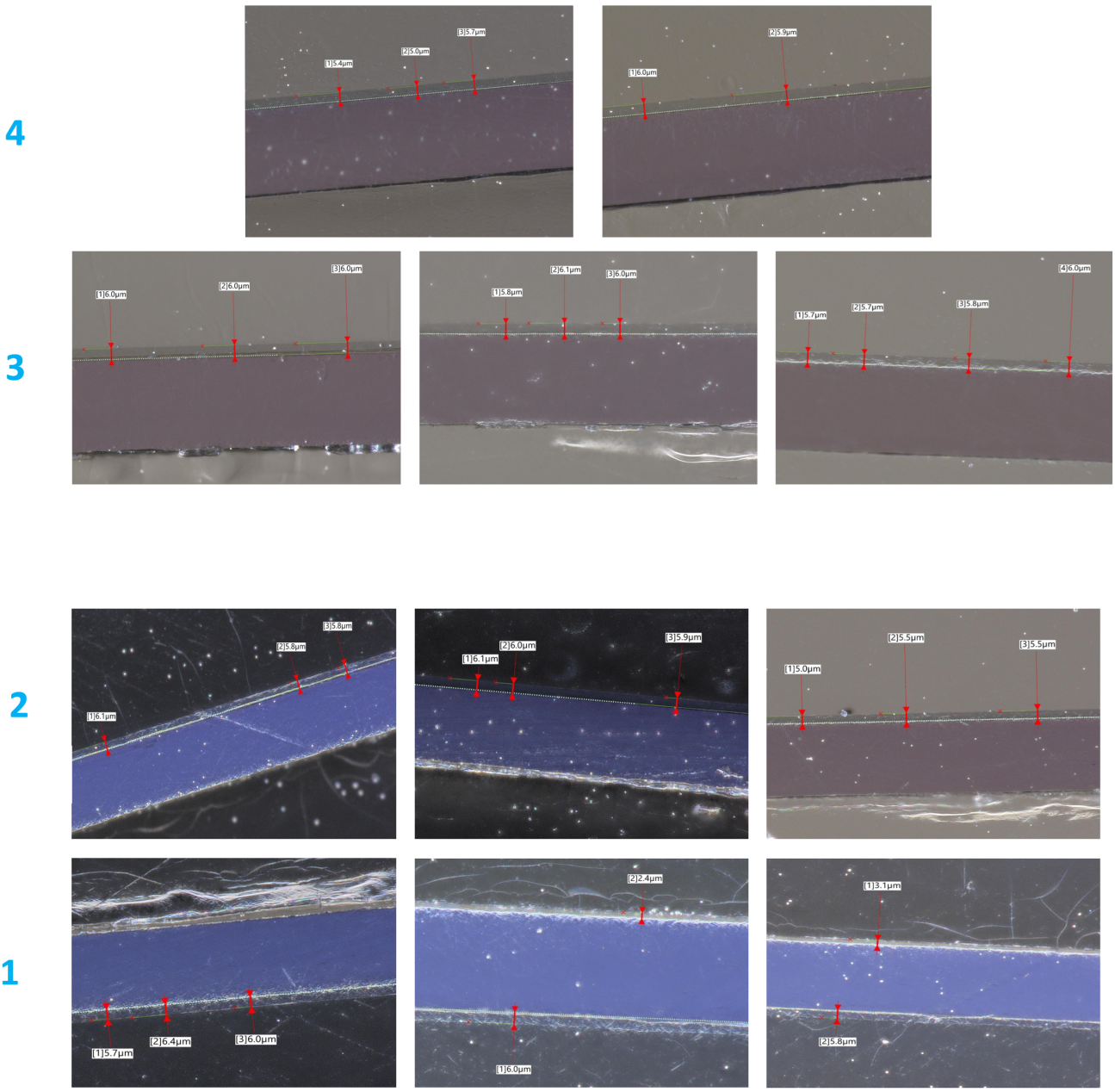

Figure D.2: Images of Cross-section at different points along the inspecting lines.